-- Electronic Supplementary Information --

Molecular Mechanism behind Cholinium-Taurate Ionic Liquid in Stabilisation of HDAC2 for Alcohol Use Disorders: Insights from DFT and MD Simulations

S. M. Esther Rubavathy,[†] Gopal Hema[†] and M. Prakash[†,*]

[†] Computational Chemistry Research Laboratory (CCRL), Department of Chemistry, SRM Institute of Science and Technology, Kattankulathur-603 203, Chengalpattu, Tamil Nadu, India.

Table of Contents

Figures

Fig. S18 The RDFs of oxygen (O1, O2 & O3) atoms $[Tau]^-$ ions, with the COM of water molecules at 0.80 and 1.00-mole fractions of ILs.

Fig. S19 Secondary Structure analysis confirms that the turn in the protein without ILs transformed into a helix.

Fig. S20 Secondary Structure analysis confirms that the helix in the protein without ILs transformed into a turn.

Fig. S21 Secondary Structure analysis confirms that the turn in the protein without ILs transformed into a helix.

Fig. S22 Secondary Structure analysis confirms that the turn in the protein without ILs transformed into a helix.

Fig. S23. The average plots of different mole fractions of ILs with ethanol

Tables

Table S1. The binding energy of the ILs -Water systems with dispersion correction by DFT studies.

Table S2. The values of the computed total electron density ($\rho(r_c)$) and the total Laplacian electron density ($\nabla 2\rho(r_c)$) for each complex.

Table S3. Chemical reactivity of the $[Cho]^+[Tau]^-$ IL systems.

Table S4. The average values of RMSD, RMSF, and Rg of apoprotein with water and different mole fractions of ILs.

Table S5. The quantity of water molecules and $[Cho]^+[Tau]^-$ ILs that accumulated on HDAC2's first solvation shell.

Table S6. The average value of the number of H-bonds between HDAC2 and different mole fractions of $[Cho]^+[Tau]^-$ IL.

Table S7. The average number of H-bonds between water and different mole fractions of $[Cho]^+[Tau]^-$ ILs.

Table S8. The average number of H-bonds between HDAC2 and water.

Table S9. The first and second peak values of RDF graphs.

Table S10. The ternary mixture of ethanol and $[Cho]^+[Tau]^-$ ILs in water containing HDAC2.

Table S11. The average values of RMSD, RMSF, and Rg of apoprotein with water, different mole fraction of ILs and ethanol.

Table S12. The dihedral angles phi and psi values for different mole fractions of IL

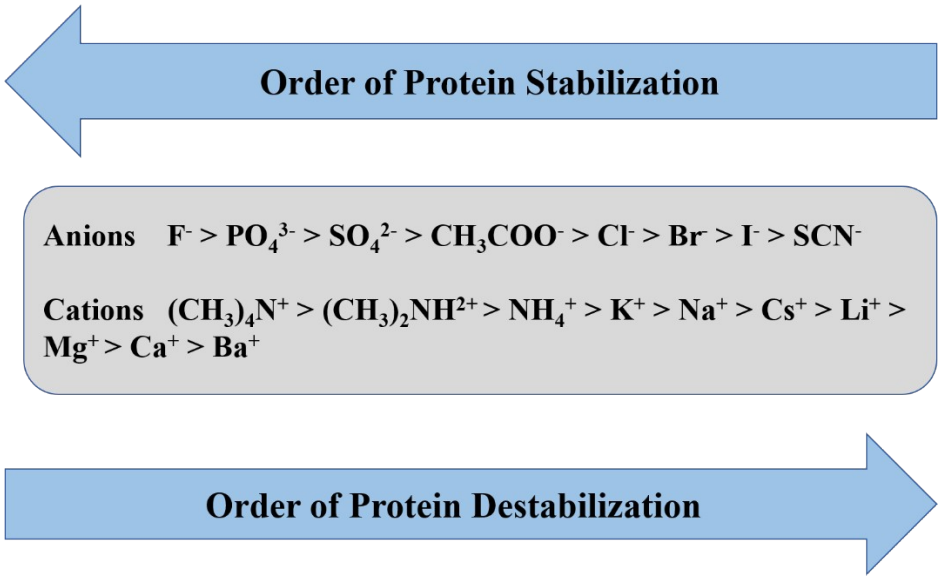

Fig. S1 Hoffmeister series of anions and cations for protein stabilisation and destabilisation.

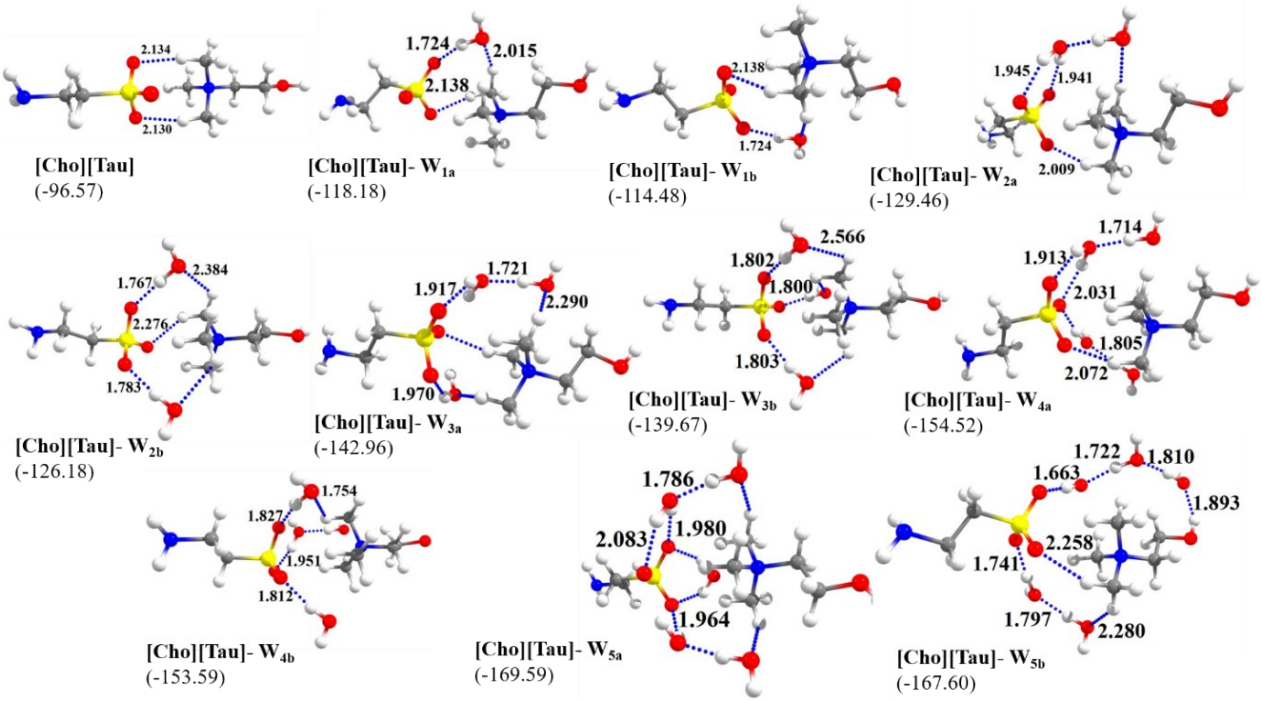

Fig. S2 Optimized geometries of the IL-water clusters with bond distances in Å.

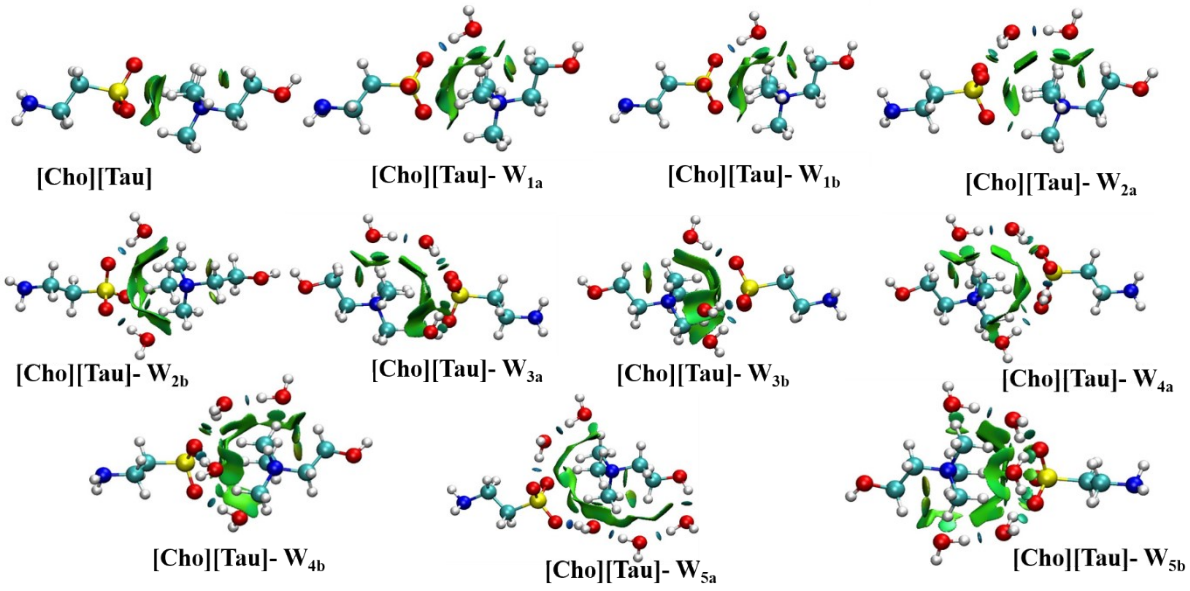

Fig. S3 NCI plots of $[Cho]^{+}[Tau]^{-}$–W_n clusters (n = 1-5), with the blue and green shaded areas denoting, respectively, strong and weak interactions.

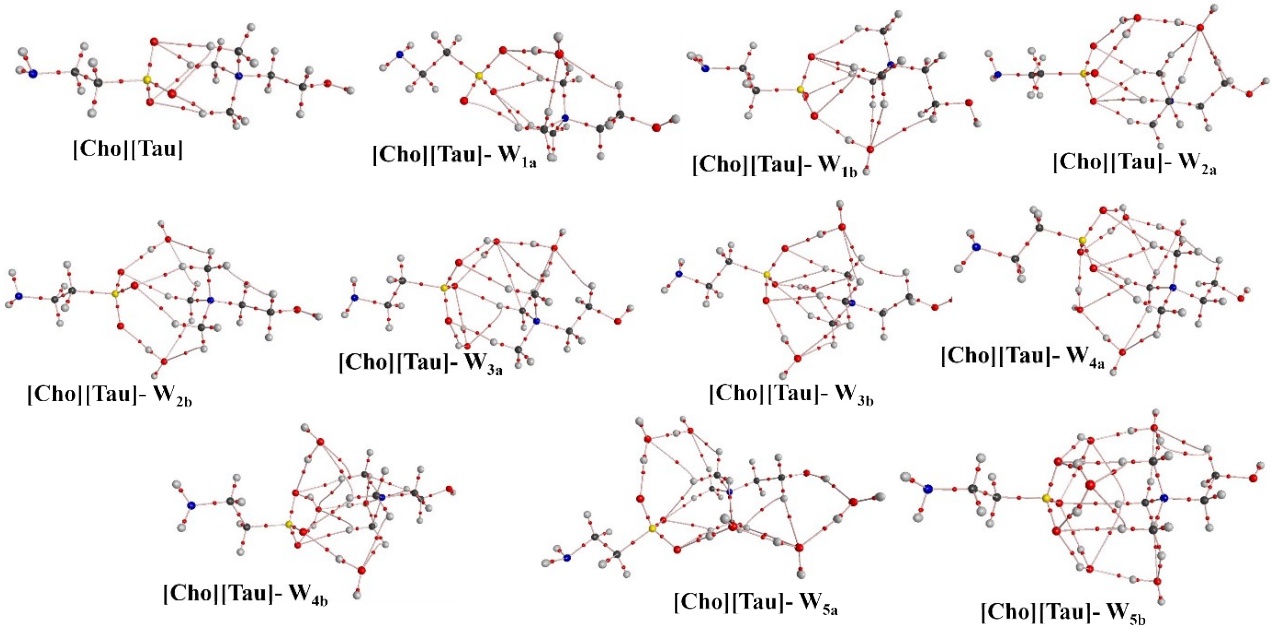

Fig. S4 AIM analysis topography of hydrated ILS clusters with isomers**.**

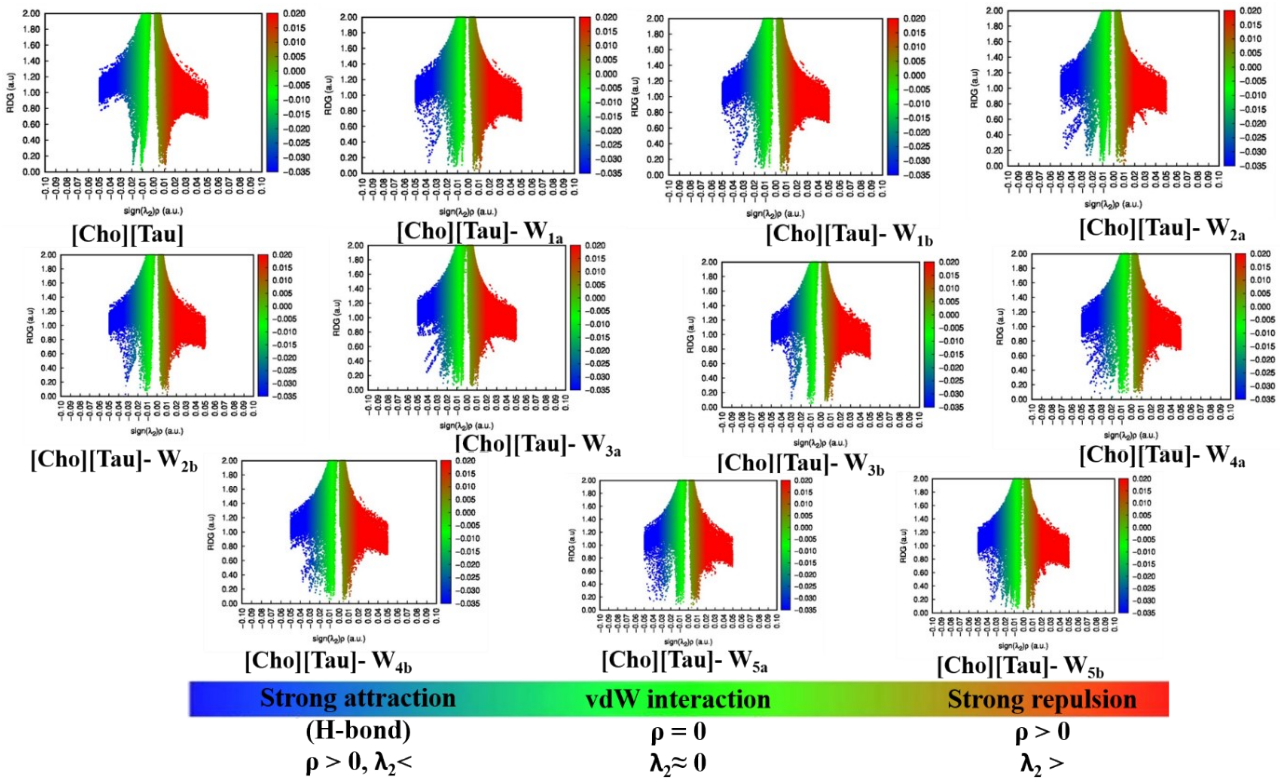

Fig. S5 RDG plots of hydrated ILS clusters with isomers**.**

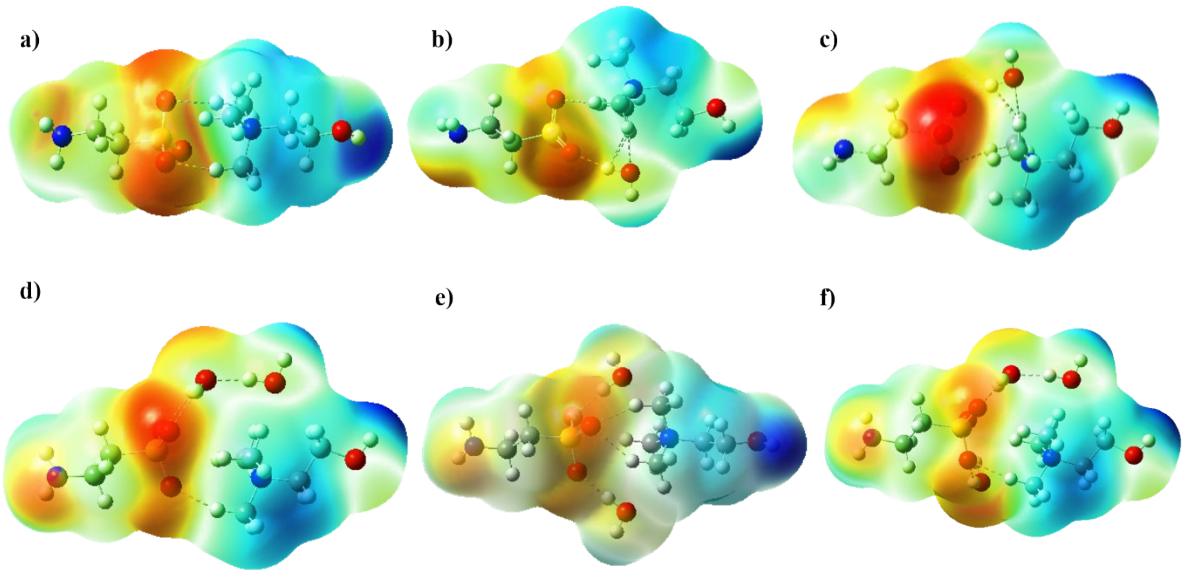

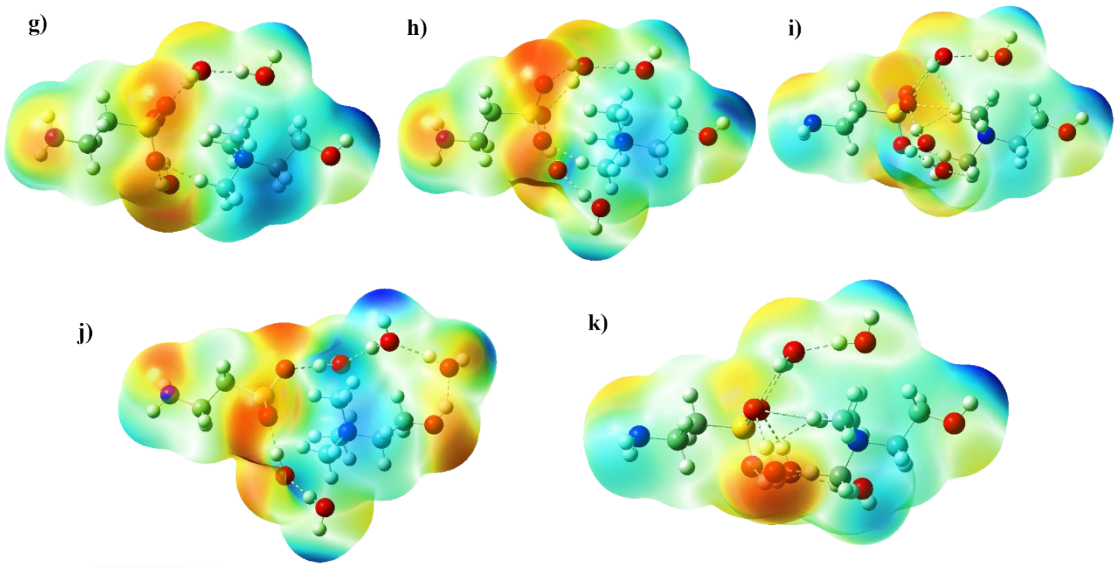

Fig. S6 MESP contour plots for a) IL-without water b)[Cho][Tau] IL- W_{1a} c) [Cho][Tau] IL- W_{1b} d) [Cho][Tau] IL- W_{2a} e) [Cho][Tau] IL- W_{2b} f) [Cho][Tau] IL- W_{3a} g) [Cho][Tau] IL- W_{3b} h) [Cho][Tau] IL- W_{4a} i) [Cho][Tau] IL- W_{4b} j)[Cho][Tau] IL- W_{5a} k) [Cho][Tau] IL- W_{5b}

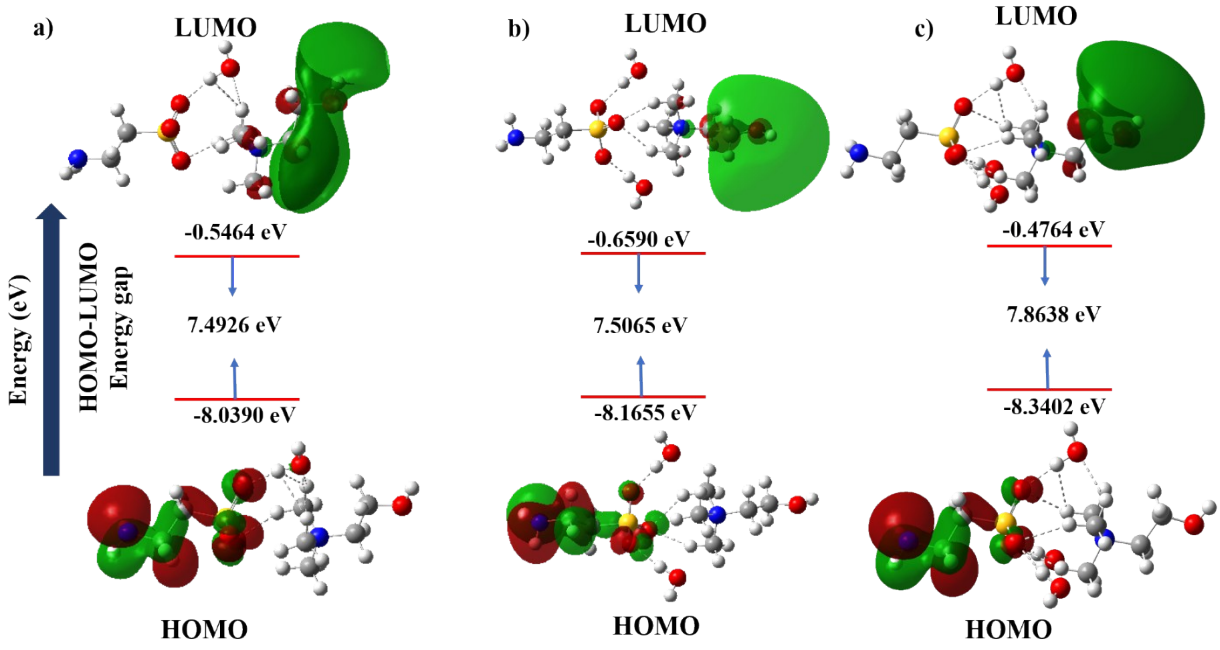

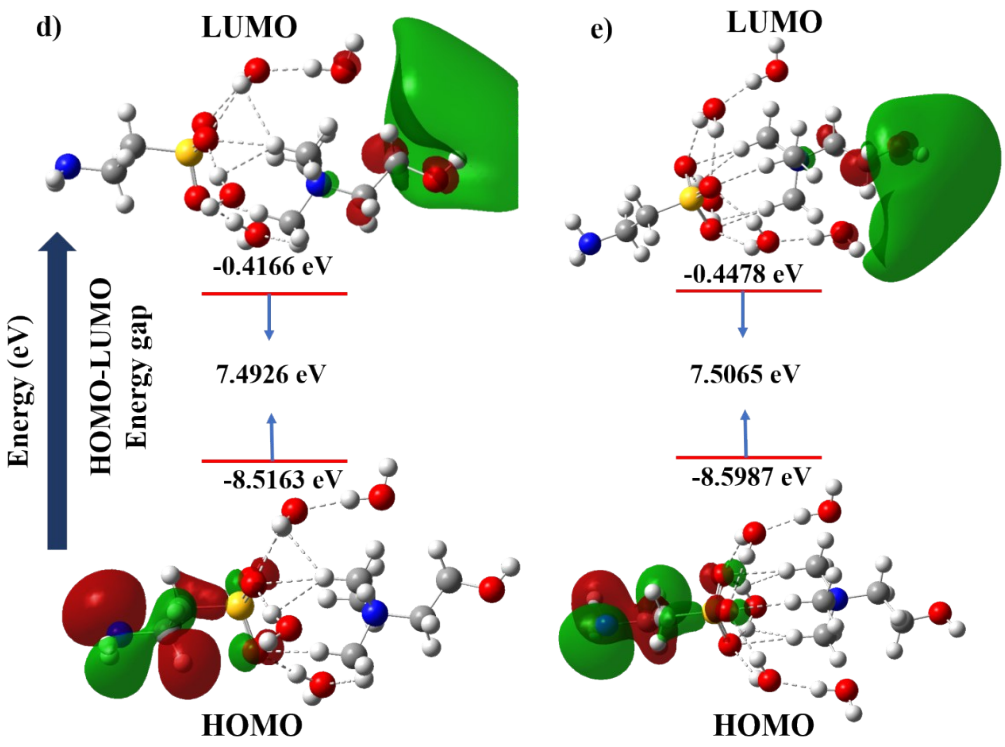

Fig. S7 FMOs including energies of HOMO and LUMO of a)[Cho][Tau] IL- W1b b) [Cho][Tau] IL- W2b c) [Cho][Tau] IL- W3b d) [Cho][Tau] IL- W4b e) [Cho][Tau] IL- W5b

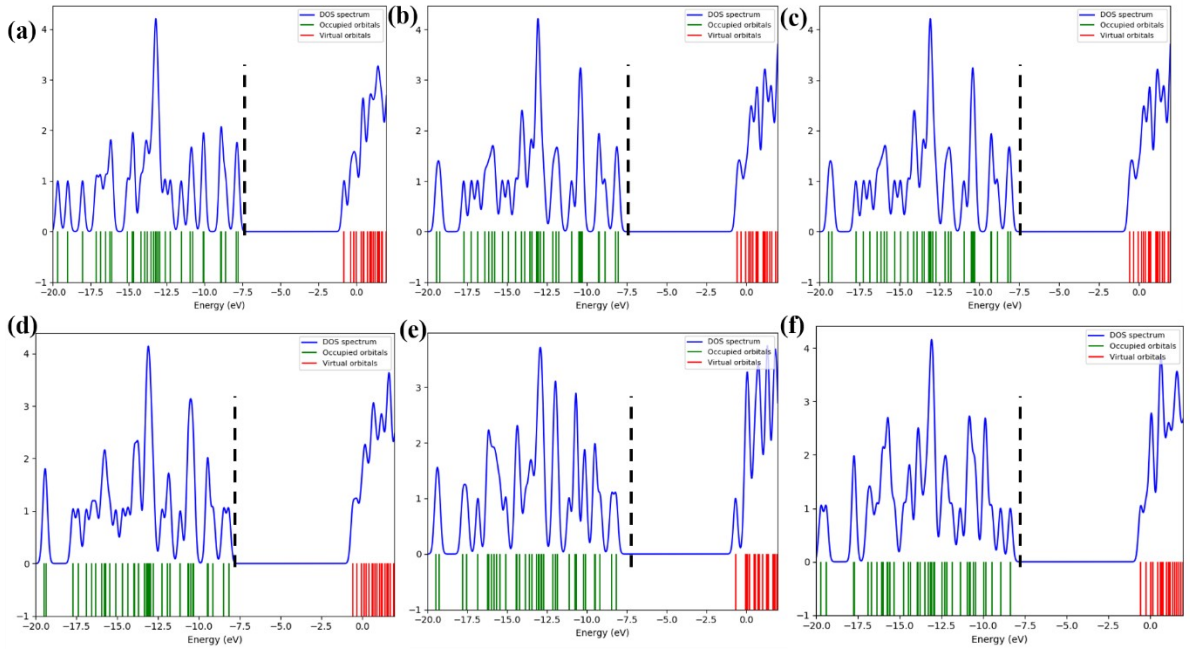

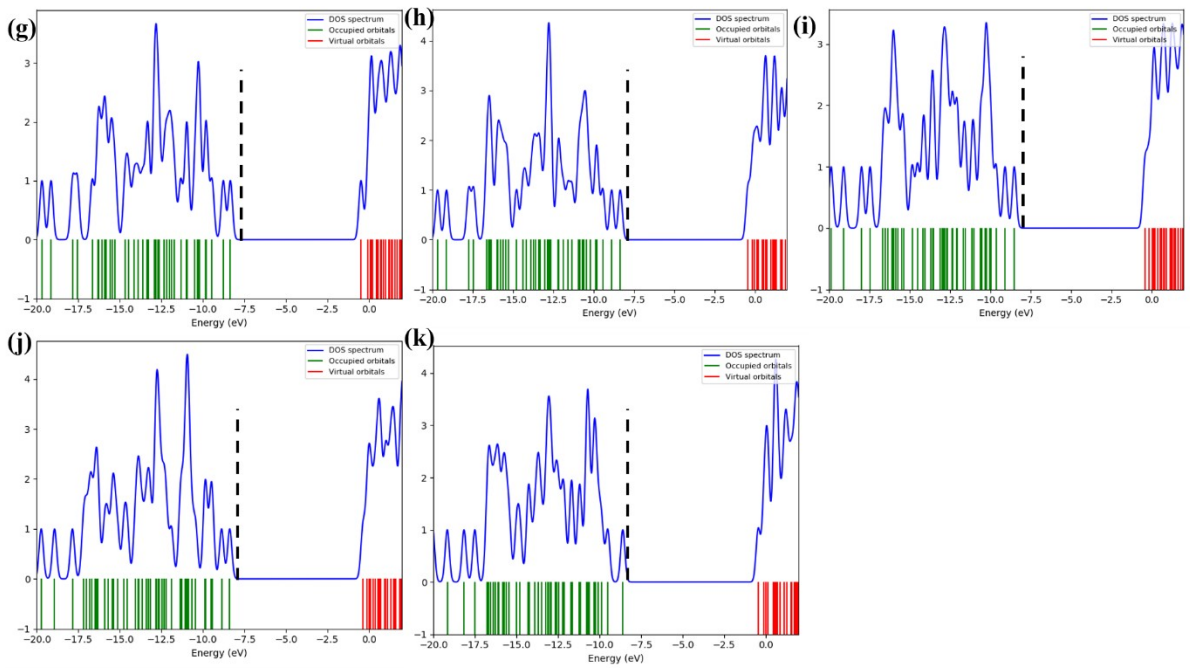

Fig. S8 DOS plots for a) IL-without water b)[Cho][Tau] IL- W1a c) [Cho][Tau] IL- W1b d) [Cho][Tau] IL- W2a e) [Cho][Tau] IL- W2b f) [Cho][Tau] IL- W3a g) [Cho][Tau] IL- W3b h) [Cho][Tau] IL- W4a i) [Cho][Tau] IL- W4b j)[Cho][Tau] IL- W5a k) [Cho][Tau] IL- W5b

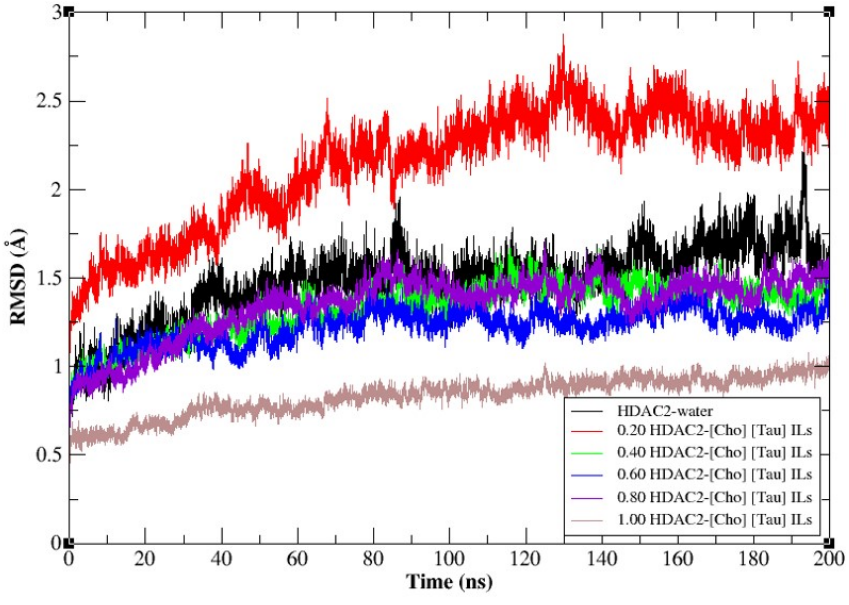

Fig. S9 RMSD plots of different mole fractions of ILs (a) Protein-water, 0.20, 0.40 and 0.60 ILs (b) 0.80 and 1.00 ILs.

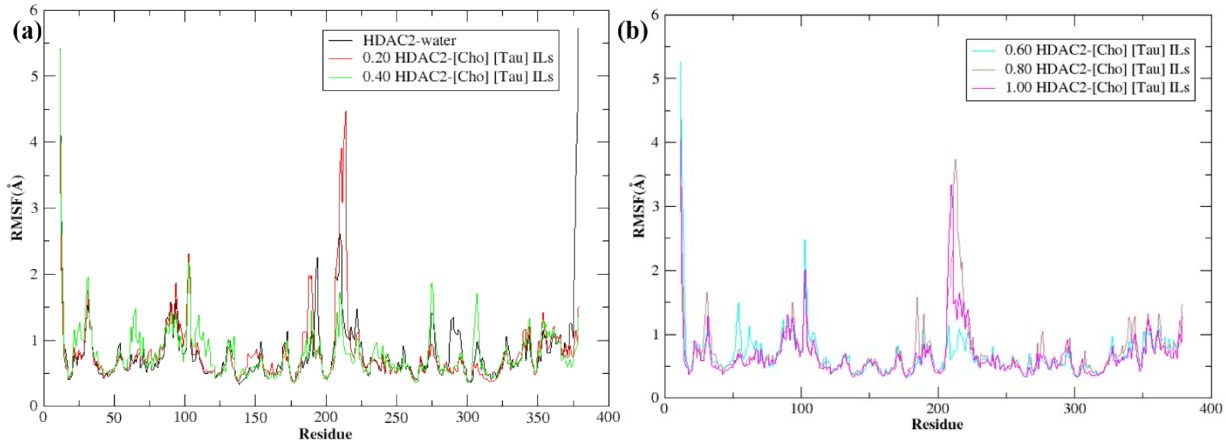

Fig. S10 RMSF plots of different mole fractions of ILs (a) Protein-water, 0.20 and 0.40 ILs (b) 0.60, 0.80 and 1.00 ILs.

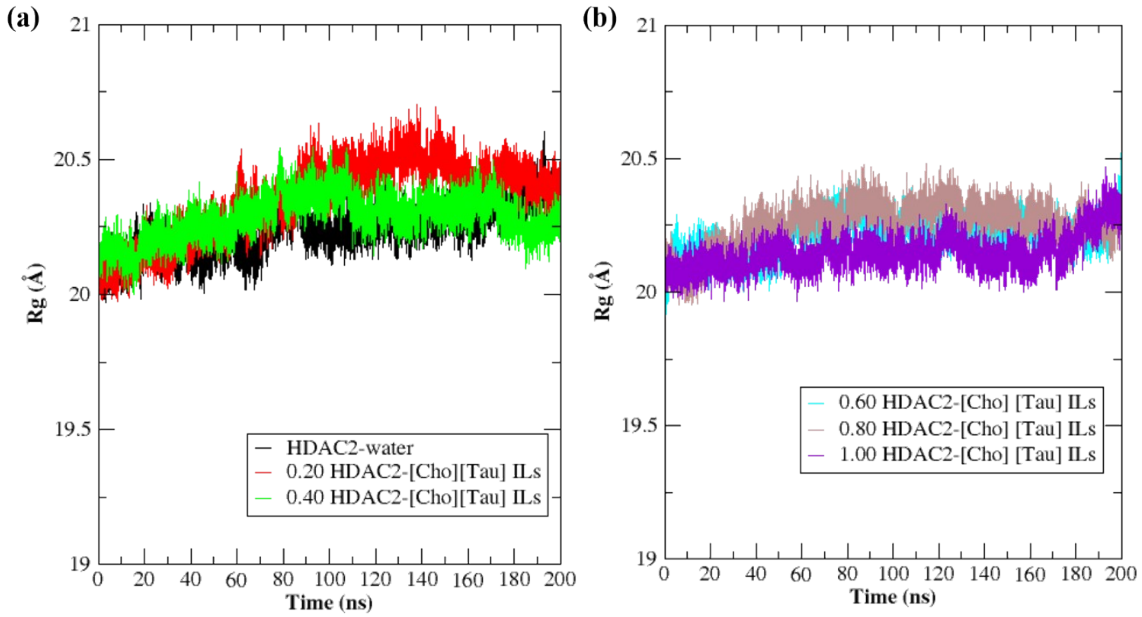

Fig. S11 Rg plots of different mole fractions of ILs (a) Protein-water, 0.20 and 0.40 ILs (b) 0.60, 0.80 and 1.00 ILs.

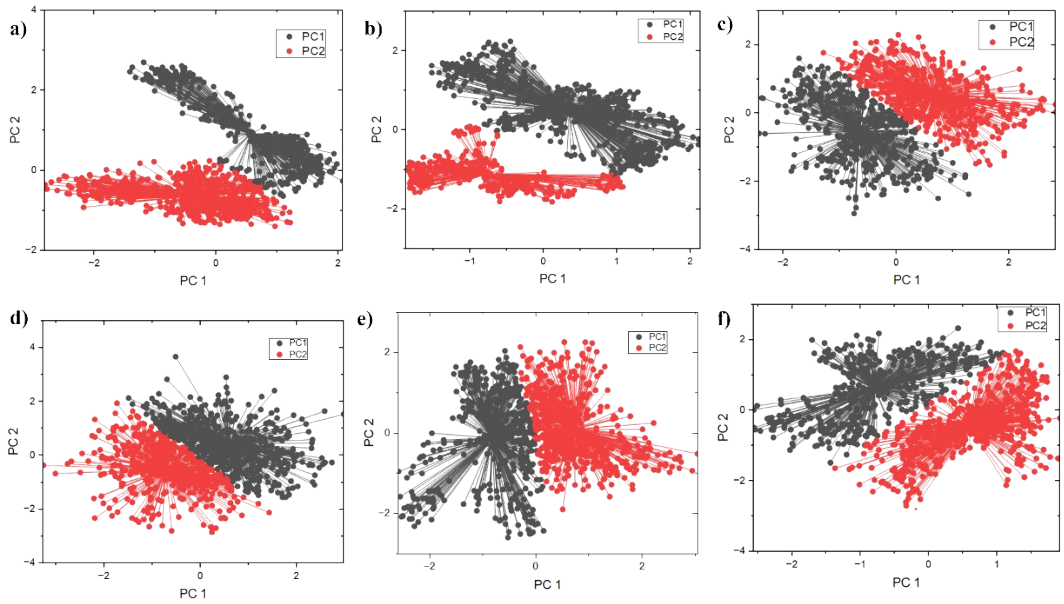

Fig. S12 PCA plots of apo-protein with different mole fractions of ILs (a) Protein-water, (b) 0.20, (c) 0.40, (d) 0.60, (e) 0.80, and (f) 1.00.

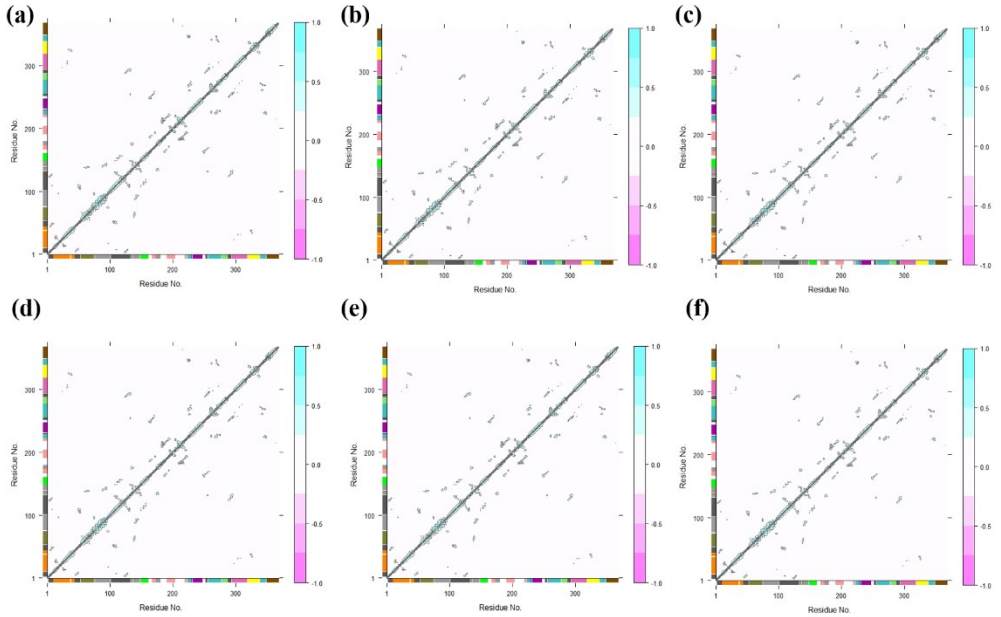

Fig. S13 DCCM plots of apo-protein with different mole fractions of ILs (a) Protein-water, (b) 0.20, (c) 0.40, (d) 0.60, (e) 0.80, and (f) 1.00.

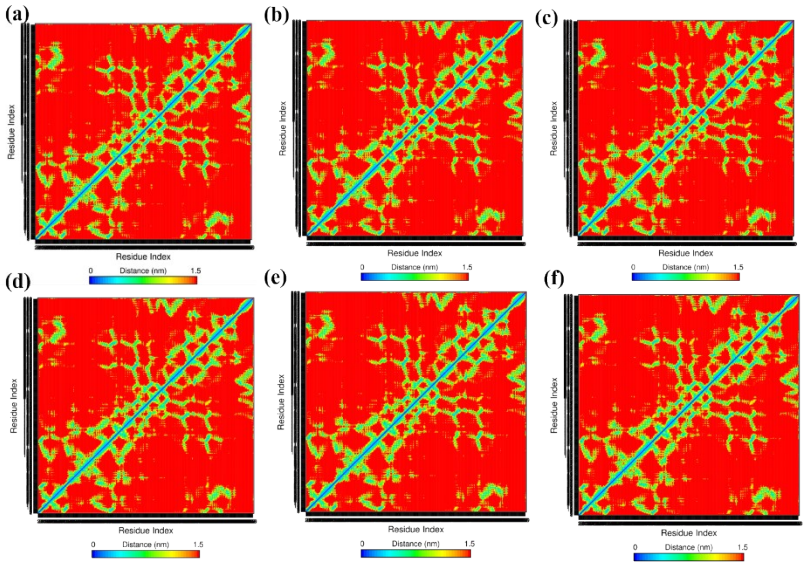

Fig. S14 Contact map plots of apo-protein with different mole fractions of ILs (a) Protein-water, (b) 0.20, (c) 0.40, (d) 0.60, (e) 0.80, and (f) 1.00.

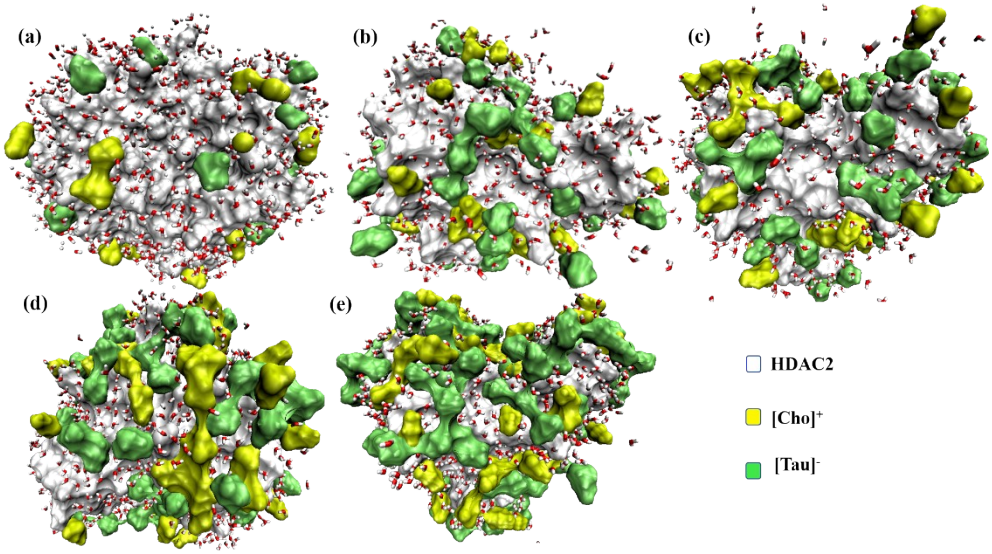

Fig. S15 The accumulation of water and $[Cho]^{+}[Tau]^{-}$ of ILs on HDAC2's first solvation shell at (a) 0.20, (b) 0.40, (c) 0.60, (d) 0.80, and (e) 1.00 mole fractions.

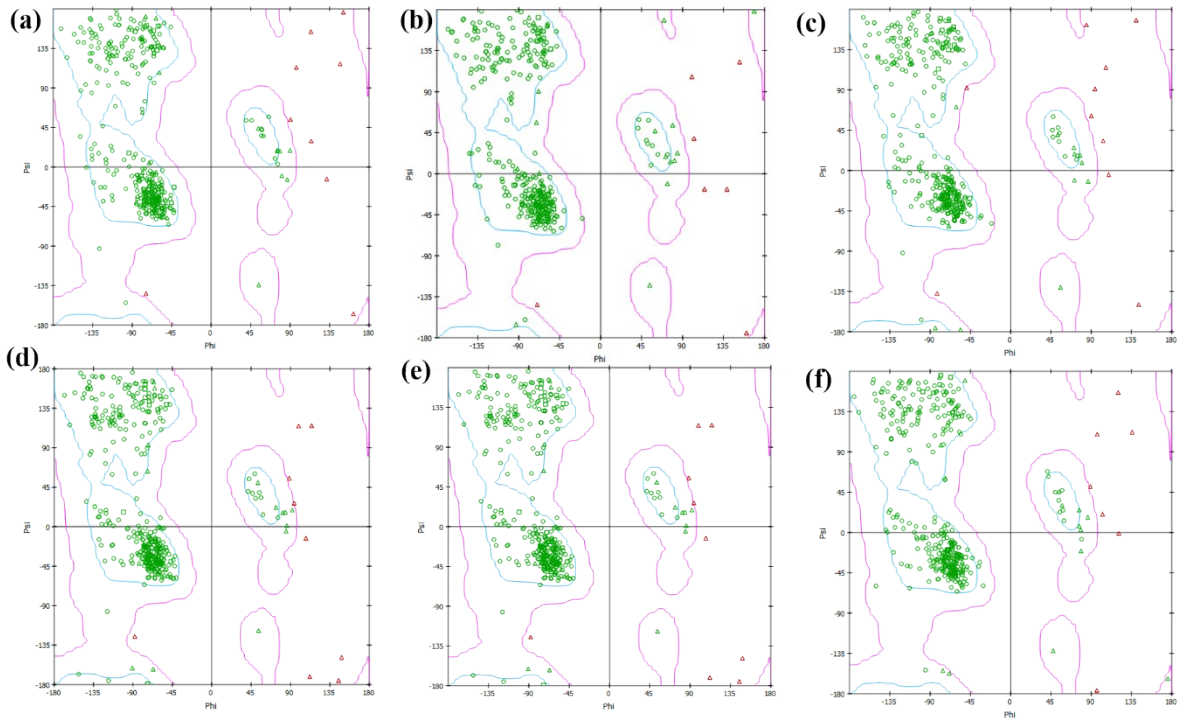

Fig. S16 Ramachandran plots of apo-protein with different mole fractions of ILs (a) Protein-water, (b) 0.20, (c) 0.40, (d) 0.60, (e) 0.80, and (f) 1.00.

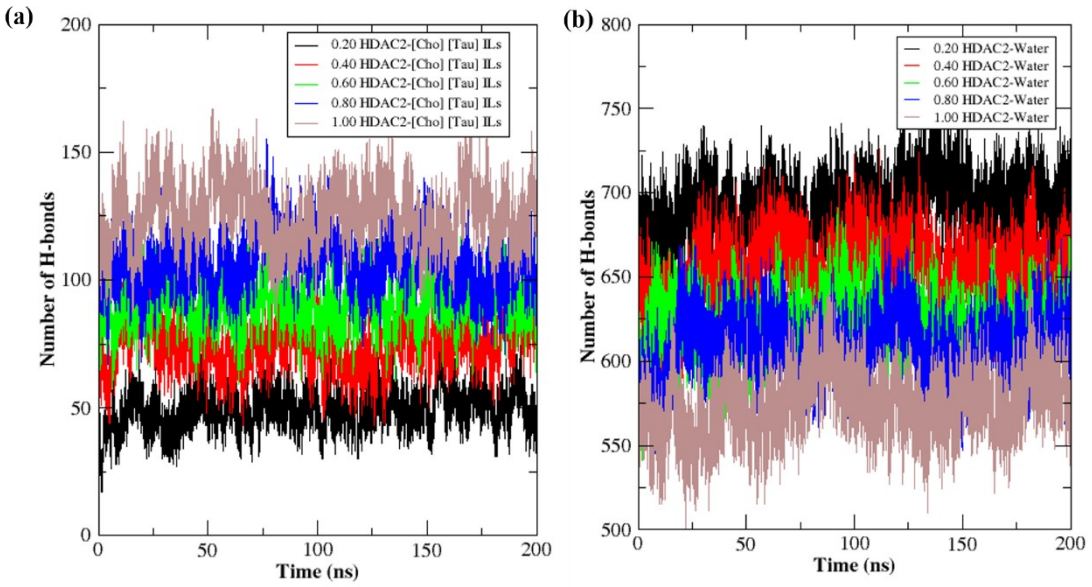

Fig. S17 The H-bonding interaction of different mole fractions of ILs a) Protein with ILs b) protein with water

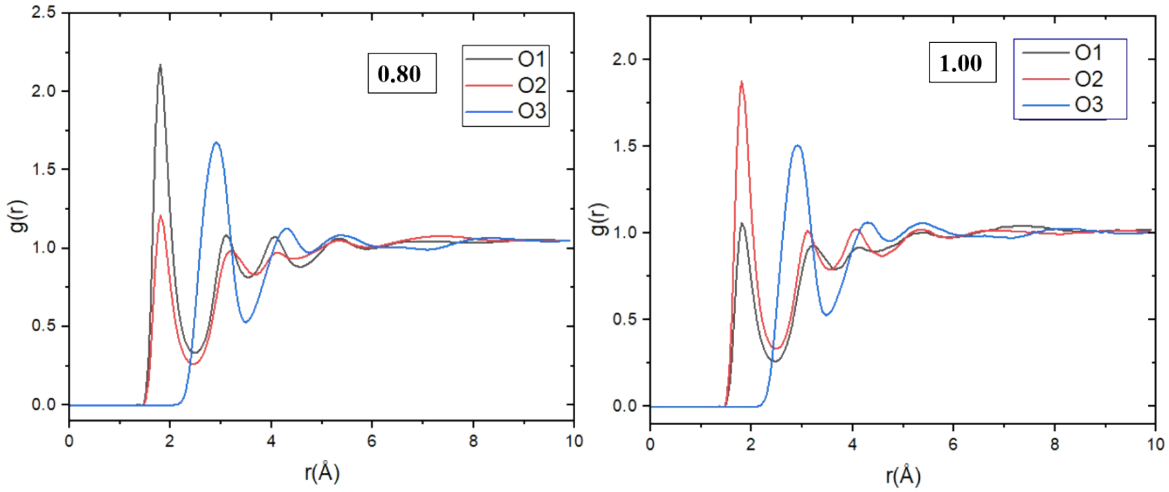

Fig. S18 The RDFs of oxygen (O1, O2 & O3) atoms $[Tau]^-$ ions, with the COM of water molecules at 0.80 and 1.00-mole fractions of ILs.

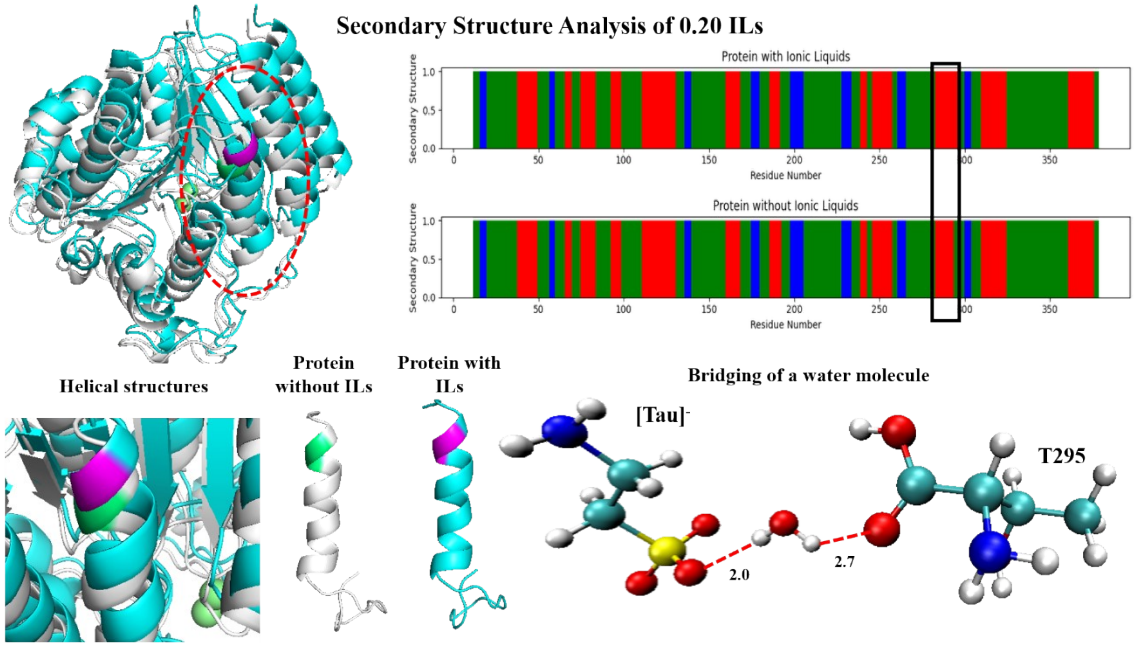

Fig. S19 Secondary Structure analysis confirms that the turn in the protein without ILs transformed into a helix.

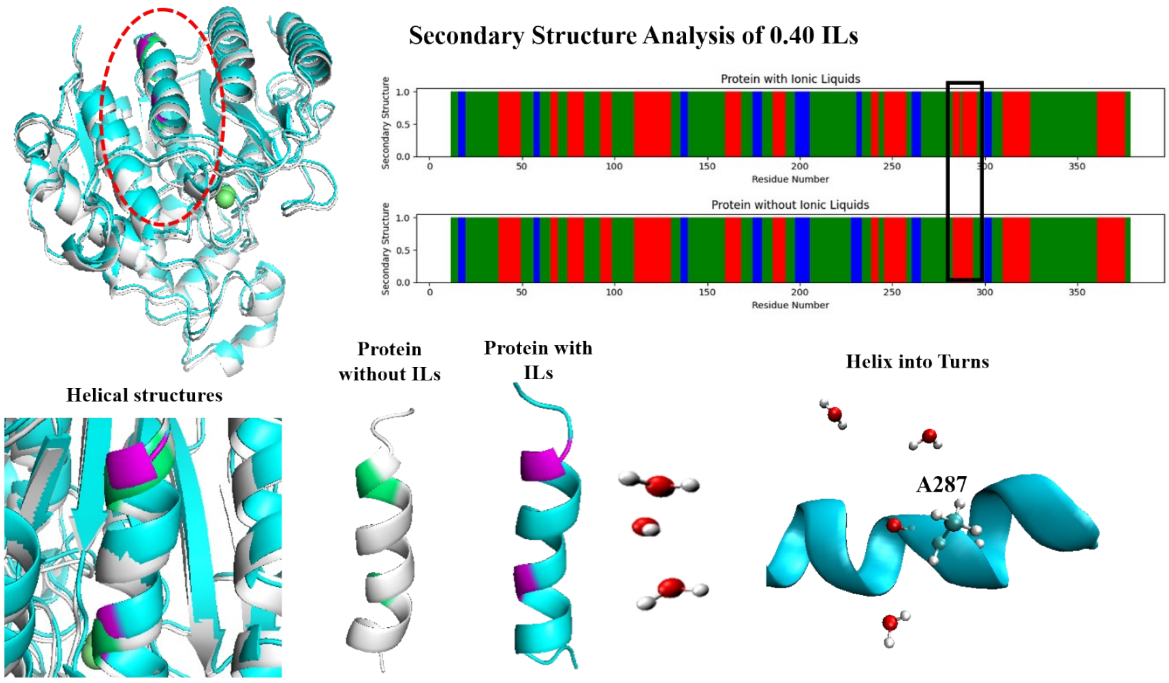

Fig. S20 Secondary Structure analysis confirms that the helix in the protein without ILs transformed into a turn.

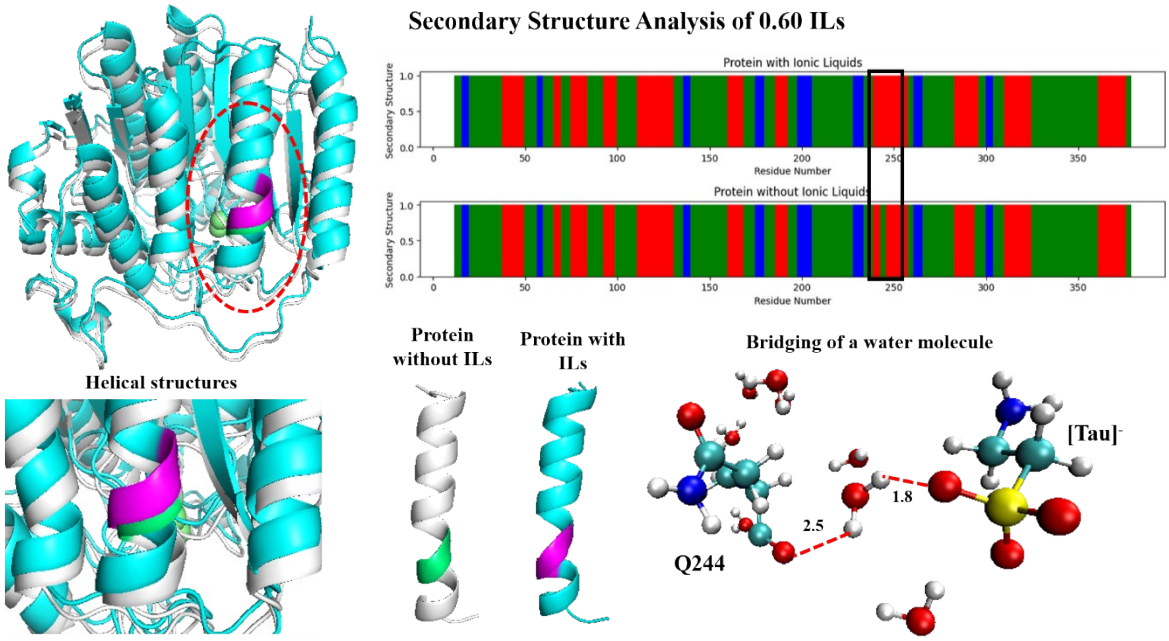

Fig. S21 Secondary Structure analysis confirms that the turn in the protein without ILs transformed into a helix.

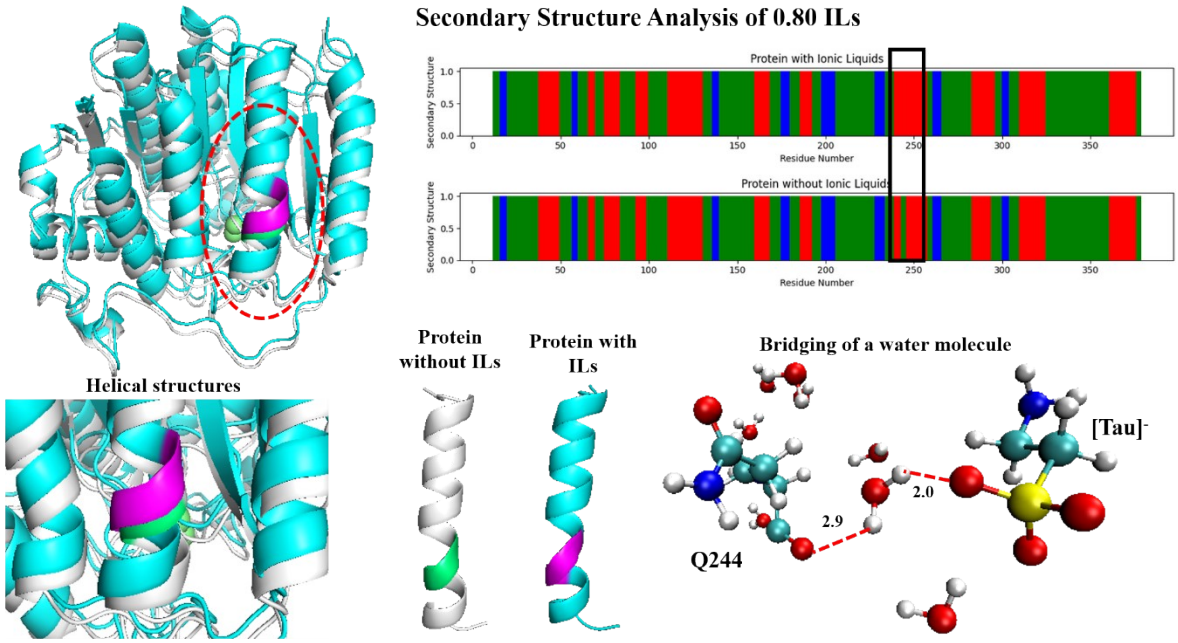

Fig. S22 Secondary Structure analysis confirms that the turn in the protein without ILs transformed into a helix.

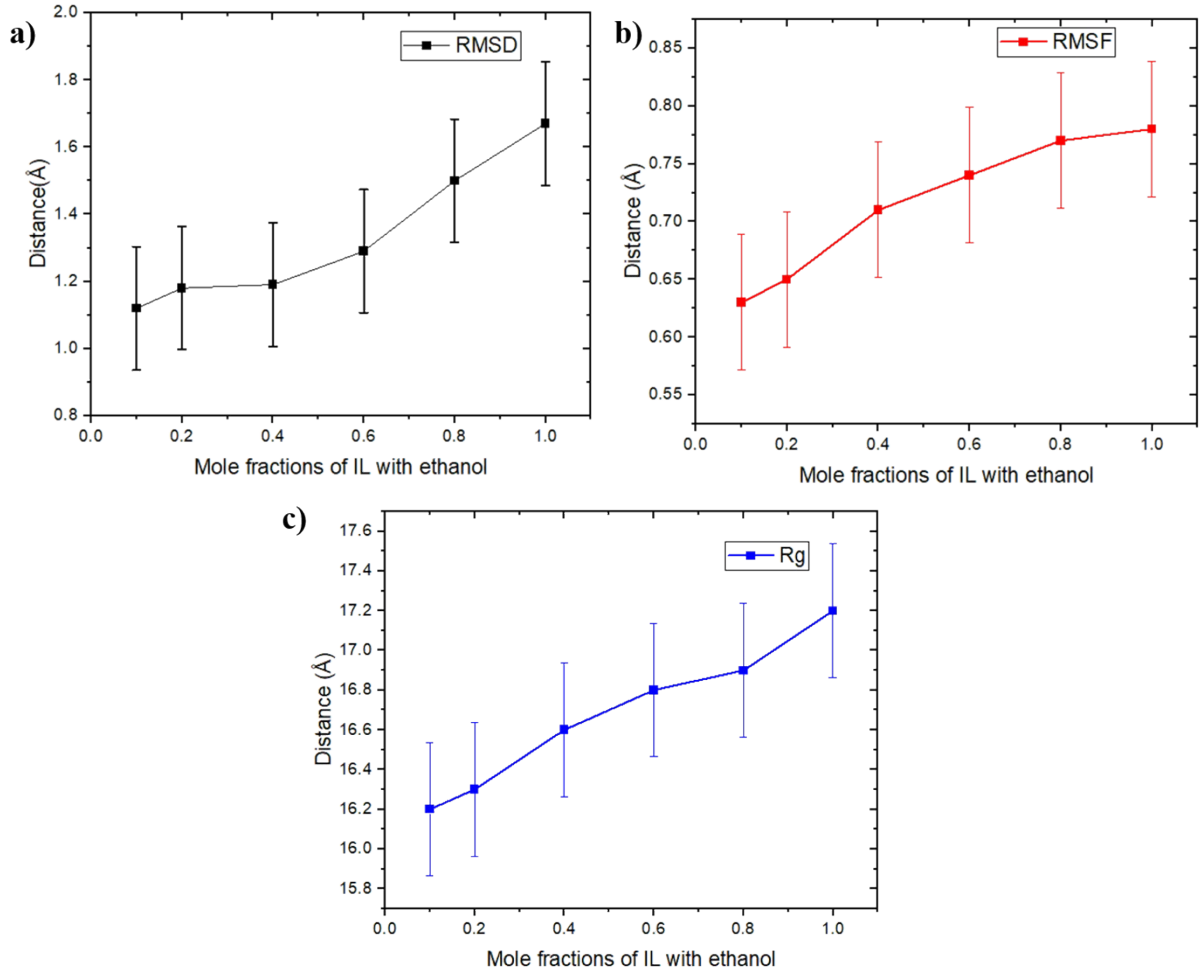

At lower mole fractions of ethanol (up to 0.40), the system maintains balanced interactions, resulting in lower RMSD values. H-bonding between ethanol and IL components stabilizes the structure. Ethanol forms H-bonds with both the $[Cho]^+$ and the $[Tau]^-$, acting as a mediator between them. The components are well-solvated, maintaining a stable configuration, resulting in low RMSD values. Over 0.60-mole fraction of ethanol can destabilize H-bonding capacity by weakening IL interaction networks. Elevated mole fractions could result in a structural reorganization, which would create ethanol–water clusters and lessen the interaction with IL ions. Molecular overcrowding effects restrict molecular mobility, leading to conformational changes and increased RMSD values.

Fig. S23 The average plots of different mole fractions of ILs with ethanol (a) RMSD plot, (b) RMSF plot, and (c) Rg plot.

Table S1. The binding energy of the ILs -Water systems with dispersion correction by DFT studies.

$W_{n=0-5}$	[Cho][Tau] IL		
	N_{HB}	M06-2X (kcal/mol)	M06-2X +D3 (kcal/mol)
n = 0	2	-95.98	-96.57
W_{1a}	3	-117.55	-118.18
W_{1b}	3	-113.55	-114.48
W_{2a}	5	-128.25	-129.46
W_{2b}	4	-125.01	-126.18
W_{3a}	6	-141.41	-142.96
W_{3b}	5	-138.13	-139.67
W_{4a}	8	-152.59	-154.52
W_{4b}	7	-151.55	-153.59
W_{5a}	10	-167.67	-169.92
W_{5b}	9	-165.46	-167.71

Table S2. The values of the computed total electron density ($\rho(r_c)$) and the total Laplacian electron density ($\nabla 2\rho(r_c)$) for each complex.

$W_{n=0-5}$	[Cho][Tau]	
	(ρ (r_c)) (a.u)	($\nabla^2\rho$ (r_c)) (a.u)
n = 0	0.0832	0.0716
W_{1a}	0.1414	0.1288
W_{1b}	0.1238	0.1132
W_{2a}	0.2073	0.1861
W_{2b}	0.1521	0.1415
W_{3a}	0.2216	0.2148
W_{3b}	0.218	0.1977
W_{4a}	0.2671	0.2457
W_{4b}	0.2361	0.2162
W_{5a}	0.3295	0.2996
W_{5b}	0.2493	0.2278

Table S3. The chemical reactivity descriptors for the IL -Water systems.

$W_{n=0-5}$	[Cho][Tau] IL										
	HOMO (eV)	**LUMO (eV)**	**Energy Gap (eV)**	**Ionization Potential (IP) (eV)**	**Electron Affinity (EA) (eV)**	**Chemical Potential (μ) (eV)**	**Hardness (η) (eV)**	**Softness (S) (eV)**	**Electrophilicity (ω) (eV)**	**Electronegativity (χ) (eV)**	**Fermi Level (E_f) (eV)**
n = 0	-7.7941	-0.7934	7.0007	7.7941	0.7934	-4.2937	3.5003	1.75017	32.2667	4.29375	-4.2937
W_{1a}	-8.0330	-0.5613	7.4717	8.0330	0.5613	-4.2971	3.7358	1.86792	34.4921	4.29715	-4.2971
W_{1b}	-8.0390	-0.5464	7.4926	8.0390	0.5464	-4.2927	3.7463	1.87315	34.5170	4.2927	-4.2927
W_{2a}	-8.1674	-0.5646	7.6028	8.1674	0.5646	-4.3660	3.8014	1.9007	36.2310	4.366	-4.366
W_{2b}	-8.1655	-0.6590	7.5065	8.1655	0.6590	-4.4122	3.7532	1.8766	36.5340	4.41225	-4.4122
W_{3a}	-8.3640	-0.5594	7.8046	8.3640	0.5594	-4.4617	3.9023	1.9511	38.8410	4.4617	-4.4617
W_{3b}	-8.3402	-0.4764	7.8638	8.3402	0.4764	-4.4083	3.9319	1.9659	38.2045	4.4083	-4.4083
W_{4a}	-8.3530	-0.4310	7.9220	8.3530	0.4310	-4.3920	3.961	1.9805	38.2031	4.392	-4.392
W_{4b}	-8.5163	-0.4166	8.0997	8.5163	0.4166	-4.4664	4.0498	2.0249	40.3955	4.46645	-4.4664
W_{5a}	-8.3792	-0.3572	8.0223	8.3792	0.3572	-4.3682	4.011	2.0055	38.2672	4.3682	-4.3682
W_{5b}	-8.5987	-0.4478	8.1509	8.5987	0.4478	-4.52325	4.0754	2.0377	41.6914	4.52325	-4.52325

Table S4. The average values of RMSD, RMSF, and Rg of apoprotein with water and different mole fractions of ILs.

S. No	Mole Fraction of ILs	RMSD (Å)				RMSF (Å)				Rg (Å)			
		Run 1	Run 2	Run 3	Average	Run 1	Run 2	Run 3	Average	Run 1	Run 2	Run 3	Average
1.	Protein-water	1.47	1.45	1.46	1.46	0.81	0.80	0.82	0.81	20.25	20.24	20.27	20.25
2.	0.20	1.63	1.10	1.54	1.42	0.80	0.87	0.67	0.78	20.22	20.21	20.23	20.22
3.	0.40	1.33	1.24	1.39	1.32	0.79	0.74	0.70	0.74	20.23	20.25	20.24	20.24
4.	0.60	1.32	1.03	1.23	1.19	0.74	0.73	0.63	0.70	20.21	20.22	20.23	20.22
5.	0.80	1.18	1.56	1.29	1.34	0.68	0.65	0.78	0.71	20.22	20.20	20.21	20.21
6.	1.00	1.19	1.18	1.16	1.17	0.66	0.69	0.68	0.67	20.14	20.12	20.13	20.13

Table S5. The quantity of water molecules and $[Cho]^+[Tau]^-$ ILs that accumulated on HDAC2's first solvation shell.

S. No	**Mole Fraction of ILs**	**Accumulation on the HDAC2 Surface**			**R$[Cho]^+$**	**R$[Tau]^-$**
		$[Cho]^+$	**$[Tau]^-$**	**Water**		
1.	0.20	21	25	3645	0.863	0.789
2.	0.40	40	45	3069	1.022	1.112
3.	0.60	51	55	2949	0.747	0.810
4.	0.80	68	71	2778	0.730	0.701
5.	1.00	82	99	2111	0.938	0.792

Table S6. The average value of the H-bonds between HDAC2 and different mole fractions of $[Cho]^+[Tau]^-$ ILs.

S. No.	Mole fractions of ILs	Number of H-bonds		
		HDAC2-$[Cho]^+$	HDAC2-$[Tau]^-$	HDAC2-$[Cho]^+$ $[Tau]^-$
1.	0.20	19.20	32.52	41.64
2.	0.40	20.40	48.94	64.95
3.	0.60	21.90	59.70	80.73
4.	0.80	24.90	69.93	94.85
5.	1.00	29.32	81.54	110.48

Table S7. The average number of H-bonds between water and different mole fractions of $[Cho]^+[Tau]^-$ ILs.

S. No.	Mole fractions of ILs	Number of H-bonds		
		Wat-$[Cho]^+$	Wat-$[Tau]^-$	Wat-$[Cho]^+[Tau]^-$
1.	0.20	402.79	764.35	1025.82
2.	0.40	497.65	1476.58	1974.47
3.	0.60	705.75	2129.85	2835.65
4.	0.80	885.50	2712.95	3598.46
5.	1.00	1024.50	3212.45	4236.58

Table S8. The average number of H-bonds between HDAC2 and water.

S. No.	Mole fractions of ILs	Number of H-bonds between HDAC2-Wat
1.	0	920.43
2.	0.20	862.54
3.	0.40	810.42
4.	0.60	775.54
5.	0.80	735.67
6.	1.00	691.43

Table S9. The first and second peak values of RDF graphs.

Systems	Ions	Reference	Selection	Distance (Å)		g(r)	
				First	Second	First	Second
0.60	Tau^-	O1	Water (COM)	1.80	3.10	1.15	0.98
		O2		1.80	3.11	2.07	1.06
		O3		2.90	4.30	1.62	1.10
0.80	Tau^-	O1		1.82	3.10	2.17	1.08
		O2		1.82	3.20	1.20	1.10
		O3		2.91	4.30	1.67	1.12
1.00	Tau^-	O1		1.80	3.92	1.97	1.03
		O2		1.80	3.10	1.10	1.30
		O3		2.90	4.30	1.56	1.08

Table S10. The ternary mixture of ethanol and $[Cho]^+[Tau]^-$ ILs in water containing HDAC2.

System	Mole fraction	Ethanol	Choline	Taurate	Water
1	Pro-water	0	0	0	16366
2	Pro-ILs	0	150	150	14467
3	0.10	30	135	135	14539
4	0.20	60	120	120	14644
5	0.40	120	90	90	14790
6	0.60	180	60	60	14942

7	0.80	240	30	30	15112
8	1.00	300	0	0	15285

Table S11. The average values of RMSD, RMSF, and Rg of apoprotein with water, different mole fraction of ILs and ethanol.

System	Mole fraction	RMSD (Å)	RMSF (Å)	Rg (Å)
1	Pro-water	1.29	0.69	16.5
2	Pro-ILs	1.27	0.64	16.4
3	0.10	1.12	0.63	16.2
4	0.20	1.18	0.65	16.3
5	0.40	1.19	0.71	16.6
6	0.60	1.29	0.74	16.8
7	0.80	1.50	0.77	16.9
8	1.00	1.67	0.78	17.2

Table S12. The dihedral angles phi and psi values for different mole fractions of IL.

Mole Fractions	Residues	Conformational changes	ϕ (Phi)		ψ (Psi)		Deviations	
			Without IL	With IL	Without IL	With IL	ϕ (Phi)	ψ (Psi)
0.20	K294	Turn to Helix	-65.9°	-73.2°	-17.9°	-40.0°	-7.3°	-22.1°
	T295	Turn to Helix	-73.2°	-72.3°	-40.0°	-67.0°	-0.9°	-27.0°
0.40	A287	Helix to Turn	-83.7°	-79.4°	-9.0°	-13.1°	-4.3°	-4.1°
	K294	Turn to Helix	-65.9°	-73.7°	-17.9°	-20.7°	-7.8°	-2.8°
	T295	Turn to Helix	-73.2°	-69.7°	-40.0°	-25.5°	-3.5°	-14.5°
0.60	G243	Turn to Helix	-70.6°	-52.6°	-4.9°	-29.9°	-18.0°	-25°
	Q244	Turn to Helix	-73.7°	-73.3°	-28.6°	-45.4°	-0.4°	-16.8°
	I245	Turn to Helix	-125.8°	-115.3°	-23.2°	-22.6°	-10.5°	-0.6°
0.80	G243	Turn to Helix	-70.6°	-52.6°	-4.9°	-27.9°	-18.0°	-9.9°
	Q244	Turn to Helix	-73.7°	-71.3°	-28.6°	-45.4°	-2.4°	-16.8°
	I245	Turn to Helix	-125.8°	-115.3°	-23.2°	-22.6°	-10.5°	-0.6°
1.00	G243	Turn to Helix	-70.6°	-53.6°	-4.9°	-28.9°	-17.0°	-24.0°
	Q244	Turn to Helix	-73.7°	-72.3°	-28.6°	-44.4°	-1.4°	-15.8°

	I245	Turn to Helix	-125.8°	-114.3°	-23.2°	-21.6°	-11.5°	-1.6°